SSRG International Journal of Electrical and Electronics Engineering
ISSN: 2348-8379/ https://doi.org/10.14445/23488379/IJEEE-V12I3P118

Volume 12 Issue 3, 185-201, March 2025

Original Paper

Hybrid Controlled DVR-Based Optimization for Power Quality Enhancement in Multi-Bus Grid Systems Using Enhanced Dung Bettle Optimizer Algorithm (Enhn-DBOA)

S. Sudharani[1*], Godwin Immanuel D[2]

[1, 2]*Department of Electrical and Electronics Engineering, Sathyabama Institute of Science and Technology, Chennai, Tamil Nadu, India.*

[1*]*Corresponding Author : sudhha2221@gmail.com*

Received: 27 November 2024 Revised: 10 March 2025 Accepted: 25 March 2025 Published: 31 March 2025

Abstract - *This manuscript presents a comparative analysis of FOPID, FLC, and ANN-controlled Dynamic Voltage Restorer (DVR) systems in a grid-connected atmosphere, emphasizing the Optimization approach for enhancing performance. The Reboost converter is integrated with a DVR, and it is employed to enhance the voltage stability of a multi-bus system. The hybrid energy system consists of Photovoltaic (PV), Battery, and Wind Energy, which provides a robust interface to mitigate the voltage instability in weak bus systems. The output of the inverter is injected into the grid to compensate for the voltage sag caused by the increased load demand. To optimize control strategies, the parameters of FOPID, FLC, and ANN controllers are fine-tuned using an Enhanced Dung Bettle Optimizer Algorithm (Enhn-DBOA), providing optimal performance across a variety of operational conditions. The Dung Bettle Optimizer Algorithm (DBOA) is enhanced using the Ebola Search Optimization Algorithm (ESOA), and then it is named the Enhanced Dung Bettle Optimizer Algorithm (Enhn-DBOA). The FOPID, FLC, and ANN-controlled DVR systems are modeled in MATLAB/Simulink, and simulation results for bus voltage, real power, and reactive power are examined. According to the optimization-driven methodology, the ANN-controlled DVR system outperforms the FOPID and FLC-controlled systems in time-domain performance, with faster response times, higher voltage stability, and superior compensation for voltage sags. This paper emphasizes the effectiveness of optimization strategies in boosting DVR control performance for grid-connected systems.*

Keywords - *Dynamic Voltage Restorer (DVR), Power Quality (PQ), Artificial Neural Networks (ANN), Fractional Order PID (FOPID), Fuzzy Logic Controllers (FLC), Static VAR Compensators (SVCs).*

1. Introduction

In electrical networks, the DVR is an essential PQ tool that reduces voltage sags, swells, and harmonics. It ensures a constant power supply by injecting compensatory voltage during disruptions, improving system stability. DVRs constantly modify voltage levels to preserve operating efficiency, making them extremely effective at managing heavy load demands. Sensitive load protection and grid dependability are greatly enhanced by their quick response and sophisticated control techniques. High PQ is essential for reliable and effective energy distribution in contemporary grid-connected systems. The performance of delicate electrical loads is greatly impacted by voltage disturbances such as sag, swell, harmonics, and reactive power imbalances. To lessen these disruptions, a variety of power compensation tools have been used, including DVRs and SVCs. DVRs have become well-known because of their efficient voltage injection and fluctuation stabilization capabilities. However, inefficient control algorithms frequently limit the performance of typical DVRs, resulting in problems including delayed response time, excessive steady-state error, and insufficient compensation under dynamic grid settings. Furthermore, a lot of DVR solutions currently in use rely on conventional controllers like PI, PID, or fuzzy logic systems based on heuristics, which have trouble providing adaptive real-time performance under different load scenarios. Although several optimization techniques were developed to improve DVR control, current methods still have difficulty striking a compromise between fast transient response and low harmonic distortion. Traditional tuning strategies, such as gradient-based and heuristic optimization techniques, frequently have early convergence to local optima, which reduces their usefulness. Furthermore, intelligent-based controllers such as ANN, FOPID, and FLC have been investigated for DVR applications. These approaches, however, offer some drawbacks, such as large computing overhead, poor learning rates, and trouble implementing in real time. Although they can learn adaptively, ANN-based controllers are not feasible for dynamic grid settings since they need large training datasets and a lot of processing power.

Scalability and adaptability in complex power systems may be limited by FLC controllers' reliance on expert knowledge for rule definition. Advanced control strategies are required to maintain grid stability because integrating RES, like wind and solar PV, introduces additional power fluctuations. A significant research gap still exists in the form of an ideal, adaptable, and dependable DVR control method that guarantees less Total Harmonic Distortion (THD), faster response times, and enhanced voltage stability. To overcome these difficulties, this manuscript suggests an improved DVR control approach that integrates intelligent-based controllers as best it can while avoiding their drawbacks.

To overcome these difficulties, this manuscript proposes a hybrid control strategy for DVRs that combines ANN-based techniques, FLC, and FOPID. An Enhn-DBOA is used to optimize the control parameters, and the ESOA is used to refine the results further. This innovative optimization framework greatly enhances voltage compensation capabilities, reduces response time, and permits real-time flexibility. A Reboost converter also improves the system's supply of a steady DC-link voltage, which guarantees better correction for harmonics and voltage sags in a grid-connected hybrid energy system. The proposed methodology's improved performance in PQ enhancement and voltage stability across a range of operational conditions is demonstrated through simulations based on MATLAB/Simulink.

1.1. Contribution and Novelty

- The main contribution of this manuscript is developing a comparative analysis framework for FOPID, FLC, and ANN-controlled DVR systems integrated with a Reboost converter to improve voltage stability in grid-connected multi-bus systems.
- The manuscript is significant because it uses an Enhn-DBOA, which is then refined using the ESOA, to fine-tune the control parameters of the DVR systems.
- This optimized approach improves performance under various operating conditions, effectively mitigating voltage sags caused by increased load demand.
- The incorporation of a hybrid energy system that includes PV, battery, and wind energy adds a unique layer of robustness, while the ANN-controlled DVR system is shown to provide superior time-domain performance, with faster response times and better voltage stability than FOPID and FLC-controlled systems.
- The optimization and control of DVR systems for enhancing PQ in suboptimal bus grid settings are significantly aided by this investigation.

2. Literature Review

This section discusses recent research among the many studies on scene description generation utilizing deep learning and optimization. Venkatesh and P. S. Kumar [21] have approached Customers with delicate loads that require solutions for fast voltage control.

A power electronic converter drives a DVR, which protects sensitive loads from supply voltage swings. DVR was a widely used and inexpensive treatment for severe sagging and swelling. The maximal active power contribution and voltage injection define a DVR's mitigation capabilities. The DC input of conventional DVRs is batteries; however, batteries are large, expensive, and dangerous to dispose of after usage. The result is that DVRs are paid less. Increasing the DVR's VA rating by 1.5 times requires increasing the DC connection voltage and improving microgrid voltage control.

Ch.S. Kumar and Z.M. Livinsa [22] have presented a three-phase Z-Source Inverter-based DVR designed to eliminate voltage variations, sagging, swelling, and harmonics. The error-driven PID controller improves PQ performance in distribution systems by raising voltage, stabilizing it, and lowering harmonic distortion. Along with addressing other voltage issues, this technique keeps the load voltage near the nominal value. The Z-DVR's validity was demonstrated by modifying a PID controller's gain parameter using the HHO approach, comparing it to conventional and GA-based PID controllers, and performing distortion and total harmonics calculations.

P. Kumar et al. [23] have demonstrated that artificial intelligence will control a three-phase DVR. The suggested LMBP algorithm was based on supervised learning and employs an intelligent computing system. The optimized ANN model was used to calculate the fundamental load voltage components during the training process.

ANN models frequently faced the training challenges of slow system learning and getting stuck in a local optimum. By reducing error rates, the LMBP hybridized learning system gets around the previously noted problem. The ANFIS controller controls the voltage errors between the AC and DC lines. To extract the projected ANFIS models, the ANN-ANFIS-based DVR uses Gaussian membership functions and a hybrid learning technique.

The author have described a low-complexity voltage compensation management system that uses a proprietary power device called a DVR that was used with various inverter topologies. Voltage variations like sag, swell, and harmonics are reduced by a three-phase Z-Source Inverter DVR. The error-driven PID controller improves PQ in distribution networks by boosting voltage augmentation, stability, and harmonic distortion reduction. This technique manages a range of voltage problems while maintaining the load voltage close to the nominal value. The PID controller's gain parameter was modified using the HHO approach.

A.B. Abdelkader et al. [24] described a low-complexity voltage compensation management system that employs a proprietary power device known as a DVR and is employed with various inverter topologies. To reduce voltage fluctuations, sag, swell, and harmonics, a digital video recorder is powered by a three-phase Z-Source Inverter. The error-driven PID controller raises voltage, stabilizes it, and lowers harmonic distortion to enhance PQ performance in distribution systems. This approach keeps the load voltage near its nominal value while addressing various additional voltage issues. The HHO method was used to modify the gain of a PID controller.

M. Rawa et al. [25] have demonstrated the DVR was used to address the PQ issues related to RESs. The PI controller controlled the DVR, and the GTA was used to determine the controller's gain settings for various PQ problems. Two operating modes were discussed: off-grid and on-grid with high PV, wind, and nonlinear loads. To get the intended outcome and DVR power, two comparison studies of various optimization techniques were also suggested, along with adding a second controller.

A.C. Kathiresan et al. [26] have demonstrated to solve PQ difficulties, and the PV DVR was designed for series-connected solar and wind farms. The operational zone of the recommended hybrid system was determined using graphical analysis. Solar PV electricity integration into the grid is supported by the system's performance in different grid topologies. Series voltage injection can reduce the negative impact of voltage sag and unbalance on wind-connected induction generators.

2.1. Problem Statement

The demand for robust and adaptable voltage regulation techniques to reduce PQ disturbances, including voltage sag, swell, and harmonic distortions, has grown due to modern power systems' increasing reliance on delicate electronic equipment. Although they are commonly used, traditional DVRs frequently use battery-based DC inputs, which have drawbacks in terms of size, cost, and environmental impact.

Z-source inverters, intelligent controllers (PID, ANN, ANFIS), and tuning algorithms based on metaheuristics (HHO, GTA, GA-PID, ANN-ANFIS, etc.) are some more methods that have been investigated to improve DVR performance. However, behind the dynamic response, limited voltage compensation capabilities, high harmonic distortion, and inefficient parameter tuning remain challenges for current approaches, especially in grids that combine renewable energy sources. Global convergence, computational efficiency, and real-time adaptability in DVR control schemes are also not balanced by the majority of optimization methodologies. Using an improved Reboost converter and an Enhanced Dung Beetle Optimization Algorithm (Enhn-DBOA) enhanced with an Ebola Search Optimization Algorithm (ESOA), this study suggests an Enhanced Optimization-Control Framework to address these issues.

It integrates FOPID, FLC, and ANN-controlled DVRs. This innovative framework outperforms traditional techniques in PQ enhancement, guaranteeing faster response, better voltage correction, lower THD, and increased stability for renewable-integrated multi-bus systems.

3. Proposed System

The block diagram of closed loop FOPID, FLC, and ANN controlled proposed system of `hybrid energy source with RBC and DVR is specified away on Figure 1. As the series voltage injection of the DVR is three-phase, it provides an occasion for the DVR to control the current in every bus vulnerably, which implies that combined negative and zero-sequence unbalanced voltage can be compensated. To reduce voltage stress, Re-boost converters provide an incessant input current. The output ripple voltage and overall harmonic distortion factor are kept to a minimum.

Figure 1 depicts a closed-loop circuit schematic for a re-boost converter with DVR managed by FOPID, FLC, and ANN. In this diagram, the mutually 'PMSG-based' wind turbine and PV array with Re-boost-conversion are linked at a DC bus connection, which is connected to the utility grid via the grid-side converter. The AC bus bar connects the DVR and the 3ϕ load.

3.1. Controller Design

The ANN controller is intended to provide adaptive control by learning from the DVR system's input-output relationships. In contrast to the FLC, FOPID and the ANN-based DVR controller optimize voltage injection based on real-time system activity, resulting in faster and more precise voltage adjustment.

The Design and develop three distinct control strategies:

- FOPID
- FLC
- ANN

3.1.1. Modelling of FOPID (Fractional Order PID) Controller

The FOPID controller adds two more adjustable parameters λ and μ (which are non-integer orders of derivative and integral terms) to the normal PID controller's three parameters, k_p, k_d, and k_i. Therefore, the FO PID controller's transfer function can be expressed as,

$$A(s) = k_p + \frac{k_i}{s^{\lambda}} + k_d s^{\mu} \tag{1}$$

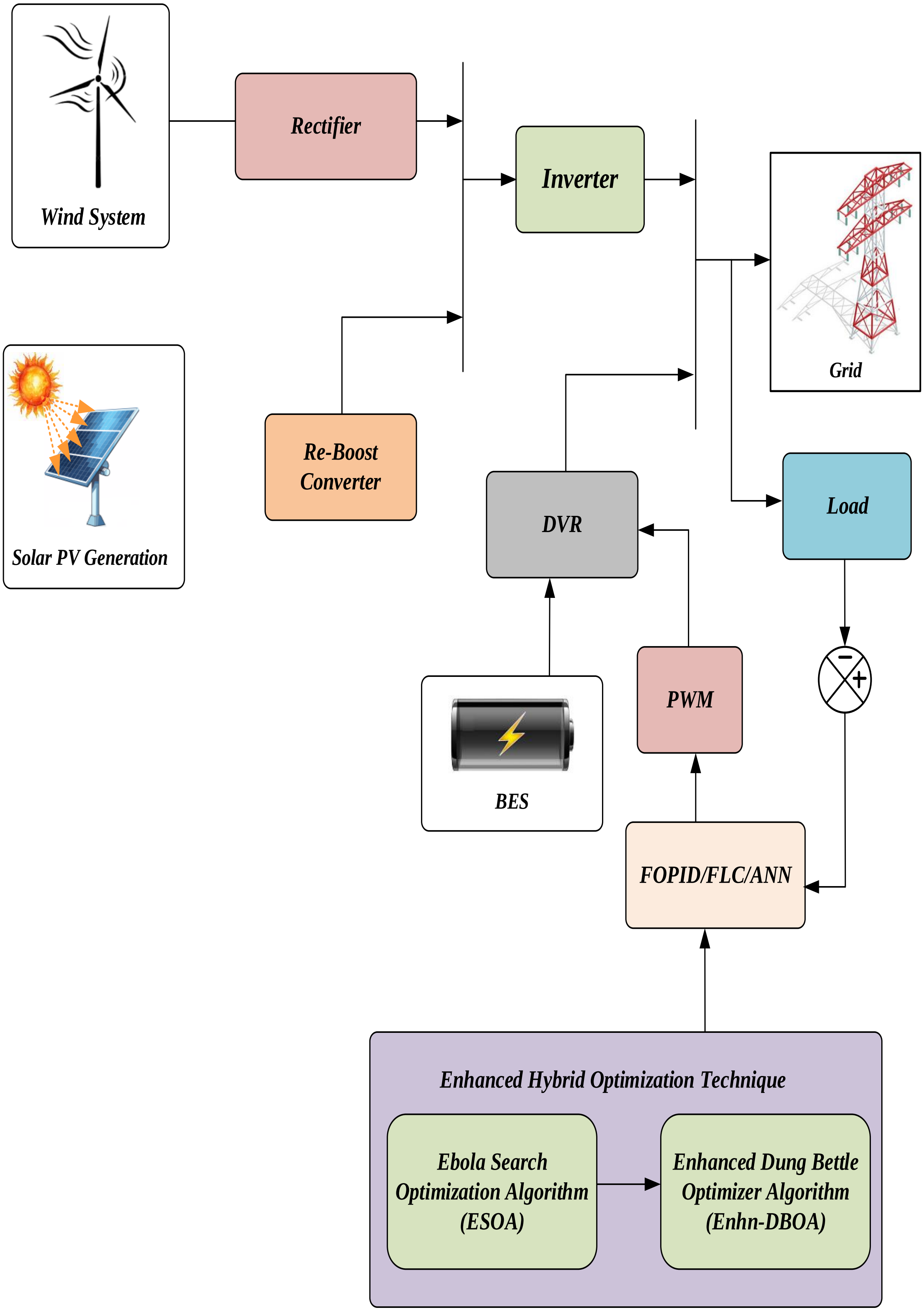

Fig. 1 Diagram of the blocks for the proposed closed-loop system

The FOPID controller's basic architecture is depicted in Figure 2. From Equation (4), we can deduce that the controller is a traditional integral PID when $\lambda = 1$ and$\mu = 1$, a proportion amplifier when $\lambda = 0$ and $\mu = 0$; a (PI) controller when $\lambda = 1$ and $\mu = 1$; and a Proportional Derivative (PD) controller when $\lambda = 0$ and $\mu = 0$. Selecting the ideal parameters to create an accurate controller is one of the main problems with FOPID controllers. An evolutionary algorithm has been used for that aim.

3.1.2. FLC Controller

Steps for FLC Modelling

Input Variables: The two key inputs are defined for FLC in the DVR system

- *Error* $(E(T))$: The difference between the measured voltage is indicated as V_{Meas}, and the reference voltage is indicated as $V_{Re\,f}$
- *Change in Error*$(\Delta E(T))$: The rate of change of the error.$\Delta E(T) = E(T) - E(T-1)$

Fuzzification

Fuzzification of input variables $E(T)$ and $\Delta E(T)$ using membership functions results in linguistic variables. Common fuzzy sets are:

- Positive Large (PL), Positive Small (PS), Positive Medium (PM), Negative Medium (NM), Negative Small (NS), Zero (ZE), and Negative Large (NL).

These fuzzy sets qualitatively describe voltage error and change.

Rule Base

The control actions are defined by the FLC using a rule base. Typically, the rules are expressed as "if-then" phrases, such as:

- If $E(T)$ is Positive Large (PL) and $\Delta E(T)$ is Negative Small (NS), then output control is Negative Medium (NM).

Inference Mechanism

The inference engine examines the rule base to determine the control action based on the fuzzified inputs. This stage maps fuzzy inputs to fuzzy outputs using methods such as Max-Min and Max-Product.

Defuzzification

After the rules are evaluated, the fuzzy output is defuzzified to create a clear control signal using techniques such as the centroid algorithm. This signal is forwarded to the DVR control system, which adjusts the inverter output for voltage sag correction.

Output Control Signal

The FLC's final output is utilized to regulate the DVR voltage injection, stabilizing the grid-connected system.

$$U(T) = F\big(E(T), \Delta E(T)\big) \tag{2}$$

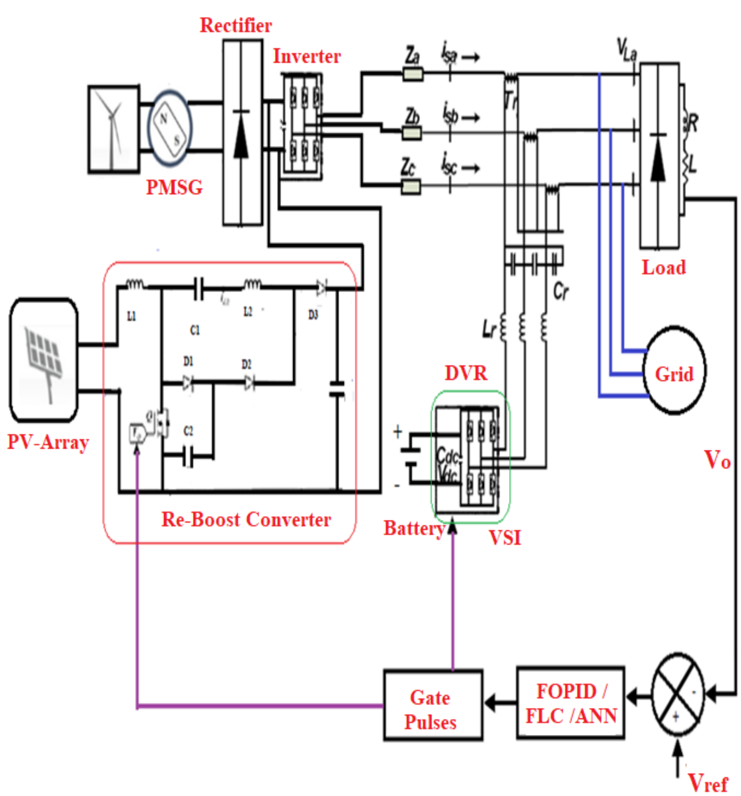

Fig. 2 Proposed circuit diagram of closed loop FOPID/ FLC / ANN controller

3.1.3. ANN Controller

Input Layer

The ANN controller employs the same inputs as the FLC, with two neurons for

- Error$E(T)$**:** Difference in reference and actual bus voltage.
- Change in error$\left(\boldsymbol{\Delta E(T)}\right)$**:** The rate at which the mistake changes.

Hidden Layer

The ANN consists of one or more hidden layers with enough neurons to learn the complex dynamics of the grid-connected system. In the deep layers, neurons use weighted sums and an activation function to process the input.

$$H_J = F\left(\sum_{I=1}^{N} \omega_{IJ}\chi_I + B_J\right) \tag{3}$$

Here, ω_{IJ} denotes the weights from the I^{th}input to theJ^{th} hidden neuron, B_J is the bias term, and $F(\cdot)$ indicates the activation function.

Output Layer

The output layer establishes a control signal for the DVR based on the processed data from the hidden layers.

$$\mu(T) = \sum_{\kappa=1}^{M} \omega_{J\kappa} H_J \tag{4}$$

The control action (voltage compensation) transmitted to the DVR inverter is denoted as $\mu(T)$

Training the ANN

The ANN is trained using supervised learning with historical data from the DVR system, and the weights are adjusted via backpropagation utilizing input-output pairs (error, change in error, control action). During the training phase, the cost function, generally called mean squared error (MSE), is minimized.

$$J = \frac{1}{\eta}\sum_{I=1}^{\eta}(\mu_{Desired}(T) - \mu_{ANN}(T))^2 \tag{5}$$

The desired control action is represented by $\mu_{Desired}(T)$, whereas the output from the ANN is represented by $\mu_{ANN}(T)$.

Adaptive Control

After training, the ANN can be employed in real-time. It learns about system dynamics and adapts to load demand and voltage variations. Alter for voltage sags, and the ANN continually modifies the control signal to the DVR.

Control Action

The DVR receives the ANN's control output to manage the voltage.

$$\mu(T) = ANN(E(T), \Delta E(T)) \tag{6}$$

3.3. Enhanced Dung Bettle Optimizer Algorithm (Enhn-DBOA) is Employed to tune the Hybrid Controller

Animal excrement serves as food for the dung beetle, a common bug in the wild. Remember that dung beetles are essential to the environment because they are found in most places of the world and function as natural decomposers. Dung beetle's ability to transfer their excrement ball as quickly and efficiently as feasible is important to note since it can keep other dung beetles from out-competing them [27].

Step 1: Initialization

In step 1, Set the input parameters to their initial values so that PV, BES, and FC are considered the input Parameters for the Dung Bettle Optimizer Algorithm (DBOA).

Step 2: Random Generation

The second phase entails creating the input parameters at random.

Step 3: Fitness Evaluation

The goal function is employed to select the fitness.

$$\mathrm{Fit(t)} = \mathrm{Mini(E)} \tag{7}$$

While Eis defined as the minimum of the error.

Step 4: Location of the Rolling Ball

The intensity of the light source is also assumed to have an impact on the dung beetle's trajectory. The dung beetle updates its position when it rolls a ball, as shown by

$$Y_I(T+1) = Y_I(T) + \alpha \times K \times Y_I(T-1) + B \times \Delta Y \tag{8}$$

$$\Delta Y = |Y_I(T) - Y^W| \tag{9}$$

When $T$is the iteration number currently in progress, $Y_I(T)$represents the $I^{th}$is denoted as dung beetle's position at the iteration ofT^{th}, $K \in (0{,}0.2)$ indicates a constant value that represents the defection coefficient, B is indicate a constant value that belongs to $(0{,}1)$, $\alpha$is a natural coefficient that is assigned -1 or 1, Y^Windicates the location that is globally worst, and ΔY simulates fluctuations in light intensity. The architecture of Enhn-DBOA is shown in Figure 3.

Step 5: Rolling Direction

To replicate the dancing action, they derive the new rolling direction using the tangent function. It's crucial to remember that just the values of the tangent function defined on the interval [0, F] are relevant. Once a new path is discovered, the dung beetle should continue rolling the ball backwards. As a result, the rolling dung beetle's definition and current position are the ensuing:

$$Y_I(T+1) = Y_I(T) + Tan(\theta)\,|Y_I(T) - Y_I(T-1)| \tag{10}$$

Here,θ is the angle of deflection, which pertains to $[0, \pi]$.

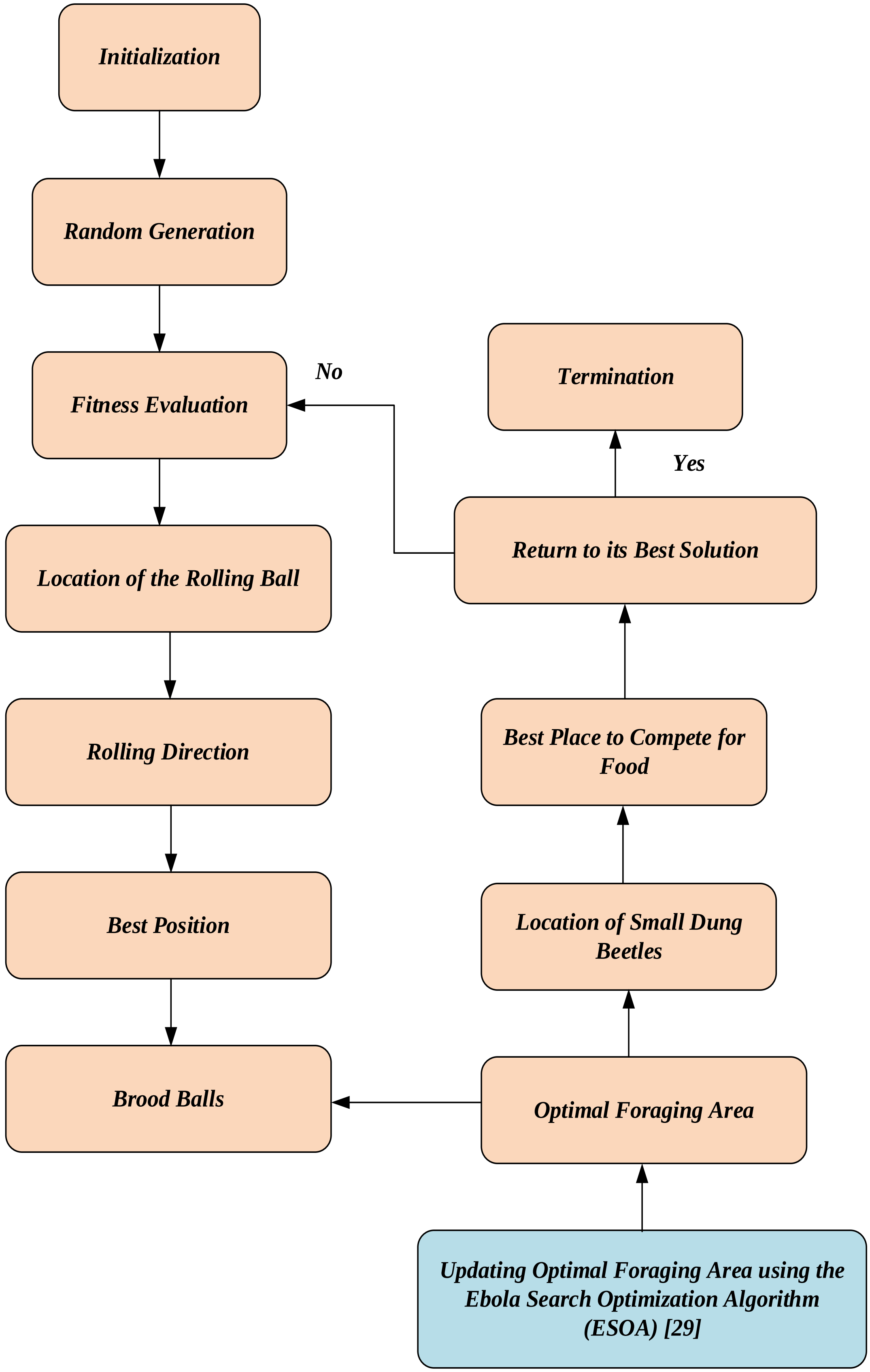

Fig 3. Architecture of Enhn-DBOA

Step 6: Best Position

Motivated by the preceding conversations, to imitate the regions delineated by female dung beetle egg-laying

$$Lower_{Bond}{}^{*} = Max(Y^{*} \times (1 - Rand), Lower_{Bond}) \quad (11)$$

$$Upper_{Bond}{}^{*} = Min(Y^{*} \times (1 - Rand), Upper_{Bond}) \quad (12)$$

When t_{Max} is indicated as the maximum iteration number, $Rand = 1 - \frac{T}{t_{Max}}$ indicates the current local best position, $Lower_{Bond}{}^{*}$and $Upper_{Bond}{}^{*}$ specifies the upper part and lower boundaries of the optimization problem, and Y^{*} indicates the current local best position.

Step 7: Brood Balls

When a sequence of iterations is followed, the placement of the brood ball is also dynamic, as dictated by

$$b_I(T+1) = Y^{*} + B_1 \times (B_I(T) - Lower_{Bond}{}^{*}) + B_2 \times (B_I(T) - Upper_{Bond}{}^{*}) \quad (13)$$

Whereby $B_I$and B_2denote two separate, size-independent random vectors $1 \times d$, where Tdenotes the magnitude of the optimization issue and $B_I(T)$ is the address data for the I^{th}brood ball at the T^{th}iteration.

Step 8: Optimal Foraging Area

In addition, to guide the foraging beetles and mimic their actual foraging habits, players must select the best feeding area. The ideal foraging area's perimeter is specifically established as follows:

$$Lower_{Bond}{}^{B} = Max(Y^{B} \times (1 - r), Lower_{Bond}) * m(i) (14)$$

$$Upper_{Bond}{}^{B} = Min(Y^{B} \times (1 - r), Upper_{Bond}) * m(i) \quad (15)$$

Here $Lower_{Bond}{}^{B}$and $Upper_{Bond}{}^{B}$ symbolize the lower and optimal foraging area. higher borders, respectively, and Y^{B}represents the global best position. The remaining parameters are specified in (84).

Step 9: Updating Optimal Foraging Area using the Ebola Search Optimization Algorithm (ESOA) [29]

Using the ESOA can improve the reliability of the DBOA in converging toward the optimal solution. Traveling and Chasing the Objective that was mentioned, the prey is hunted during the stages of exploration.

The infected person ventures outside the normal neighborhood range $Lrate$, which is the basis of the exploration phase. The present investigation considers the hypothesis that the greater the relocation distance, the more individuals $S$are exposed to infection.

$$m(i) = Lrate * Rand(0,1) + m(ind_{Best}) \quad (16)$$

According to the Equation (16), the neighborhood parameter controls the $Lrate$. If neighborhood >= 0.5, it indicates that an individual has left the neighborhood and is now in the mega infection; if the neighborhood is less than 0.5, the infection is suppressed.

Step 10: Location of Small Dung Beetles

The little dung beetle's position is updated in the following way:

$$Y_I(T+1) = Y(T) + c_1 \times (Y_I(T) - Lower_{Bond}{}^{B}) + c_2 \times (Y_I(T) - Upper_{Bond}{}^{B}) \quad (17)$$

Here, $c_1$is a randomly distributed number, $c_2$is a random vector that belongs to T^{th} (0, 1), and $Y_I(T)$is the I^{th}little dung beetle position information at the T^{th}iteration.

Step 11: Best Place to Compete for Food

Assume the region surrounding Y^{B} signifies the ideal location for food competition. The thief's position is changed during the iteration process and ca n be explained as follows:

$$Y_I(T+1) = Y^{B} + s \times G \times (|Y_I(T) - Y^{*}| + |Y_I(T) - Y^{B}|) \quad (18)$$

Wherever $G$is a regularly distributed, randomly distributed, $1 \times d$ -dimensional vector, and $s$designates a constant value. $Y_I(T)$ symbolizes the positions of $I^{th}$the thief at the T^{th}iteration. The optimal position $Y^{B}$and its fitness value are output at the end.

The DBO technique is a unique SI-based optimization strategy that consists of six fundamental processes that, for each given optimization challenge, can be expressed as:1) The DBO method and dung beetle swarm parameters were both set to zero. 2) Use the objective function to calculate each agent's fitness value. 3) Update the positions of all dung beetles. 4) Find out if an agent is beyond the boundary. 5) Revise the fitness value and current optimal solution. 6. Continue steps 1 through 6 until the requirement is satisfied. 7) Provide the fitness value and global best solution.

Step 12: Return to its Best Solution

Step 13: Termination

Verify the required stopping condition. After the maximum number of iterations, step 3 needs to be performed, and the suspension requirement is not met.

4. Result and Discussion

The proposed model was implemented with MATLAB/Simulink. The proposed system is evaluated against existing techniques such as GA-PID, ANN-AN-FIS, and HHO. The Performance matrices are evaluated using

Output voltage for FOPID, ANN, and FLC, Output voltage THD for FOPID, ANN, and FLC, RMS voltage for FOPID, ANN, and FLC, Output current for FOPID, ANN, and FLC, Output Current THD for FOPID, ANN, and FLC, Real power for FOPID, ANN, and FLC, Reactive Power for FOPID, ANN, and FLC, Compensation, Faster Response Time (s), Reactive Power Stability (%), Real Power Stability (%), Rise Time, Setting Time, Voltage Sag Mitigation, and Voltage Stability.

Table 1. Simulation parameters of integrated DVR

Symbols	Values
V_{in}	48V
C_1, C_2	10µF
C_3	180 µF
C_4	1800 µF
L_1, L_2	1µH
L_3, L_4, L_5	200mH
C_5, C_6, C_7	10µF
Frequency	50hz
Mosfet	IRF840
Diode	IN4007
Ro	80Ω
V0	475V

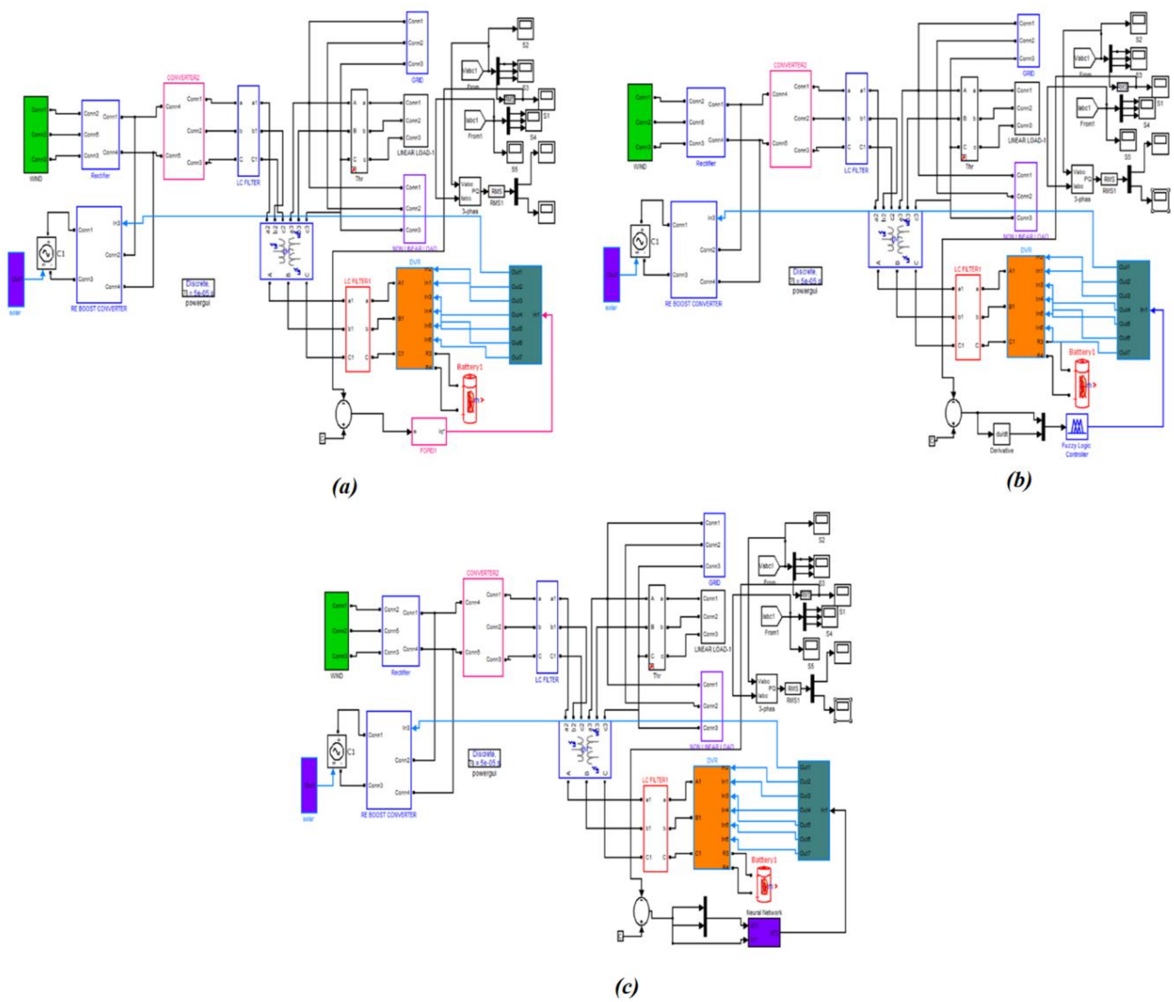

Fig. 4 Circuit diagram of Re-boost converter of DVR with closed loop for (a) FOPID controller, (b) FLC, and (c) ANN.

The circuit diagram of the Re-boost converter of DVR with closed loop for (a) FOPID controller, (b) FLC, and (c) ANN is shown in Figure 4. Performance Evaluation of Output voltage for (a) FOPID, (b) FLC, and (c) ANN is shown in Figure 5. The output voltage across the RL load and the FOPID values are marked as 470V, the value of FLC is marked as 472V, and the value of ANN is 474V. Performance Evaluation of Output voltage THD for (a) FOPID, (b) FLC, and (c) ANN is shown in Figure 6. The Output voltage THD for RL load values for FOPID is marked as 5.11%, FLC is marked as 2.96%, and ANN is marked as 2.20%.

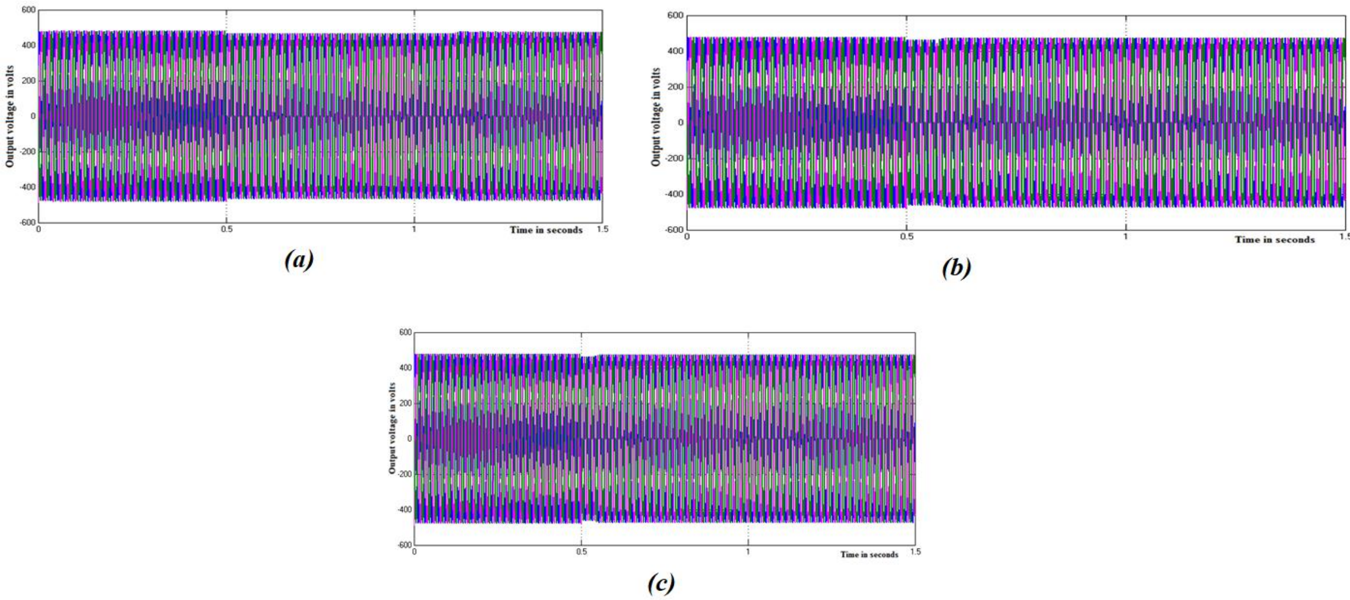

Fig. 5 Performance evaluation of output voltage for (a) FOPID, (b) FLC, and (c) ANN.

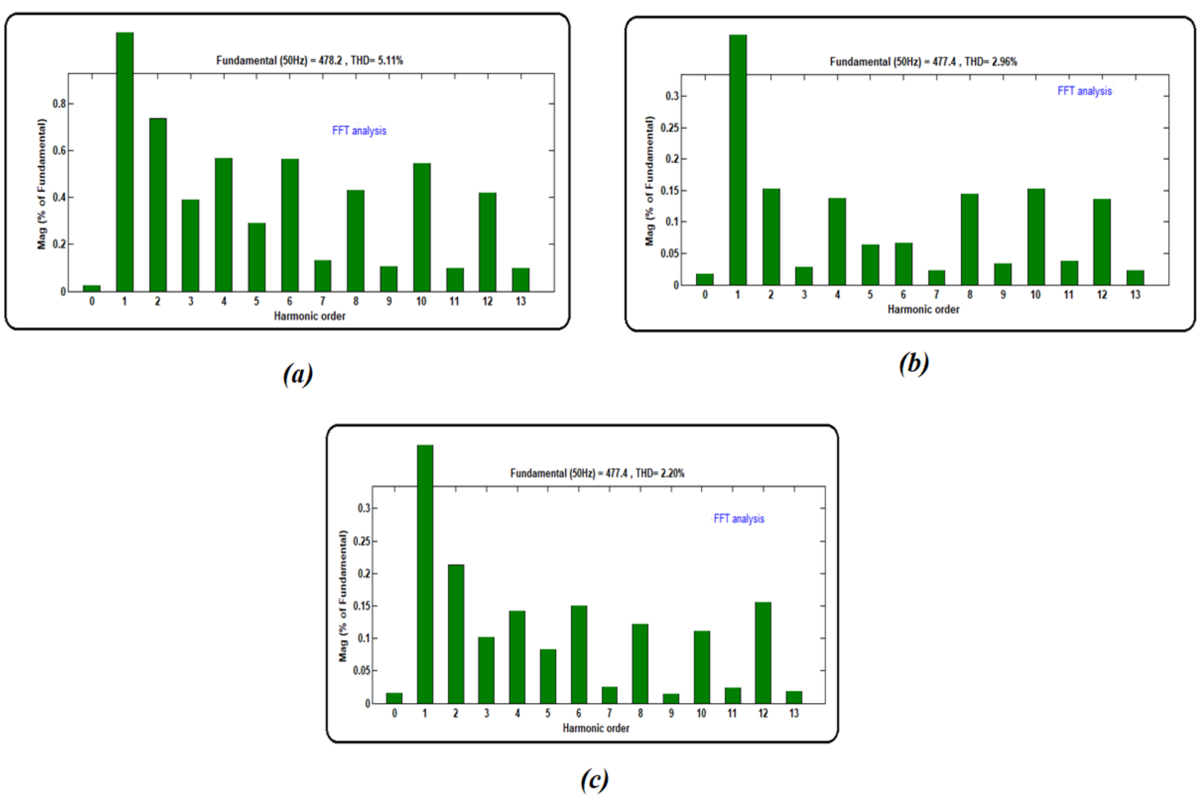

Fig. 6 Performance evaluation of output voltage THD for (a) FOPID, (b) FLC, and (c) ANN.

Figure 7 shows a performance analysis of RMS voltage for (a) FOPID, (b) FLC, and (c) ANN. The output RMS voltage for FOPID is marked as 345V, FLC is marked as 342V, and ANN is marked as 340V. Analysis of Output current for (a) FOPID, (b) FLC, and (c) ANN is shown in Figure 8. The Output current through RL load and its range is FOPID is marked as 3.4A, FLC is marked as 3.3A, and ANN is marked as 3.2A.

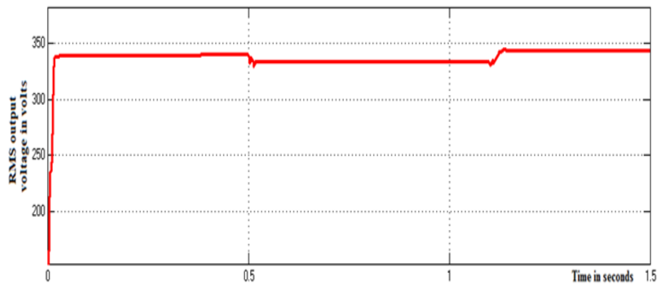

(a)

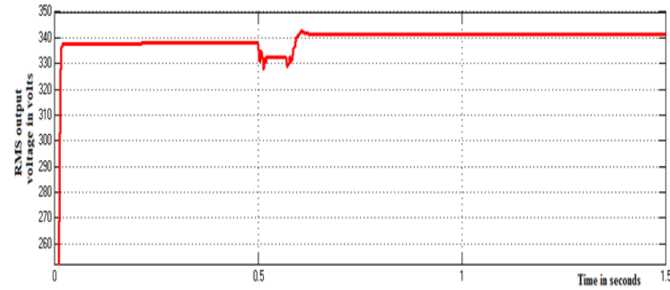

(b)

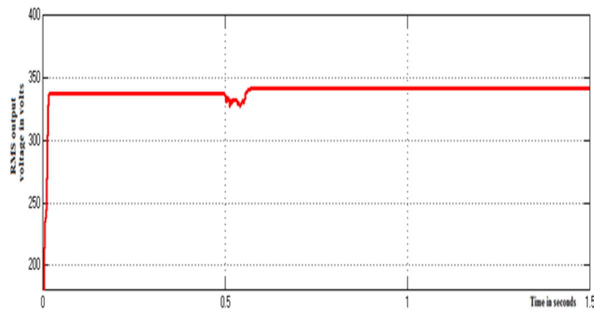

(c)

Fig. 7 Performance analysis of RMS voltage for (a) FOPID, (b) FLC, and (c) ANN.

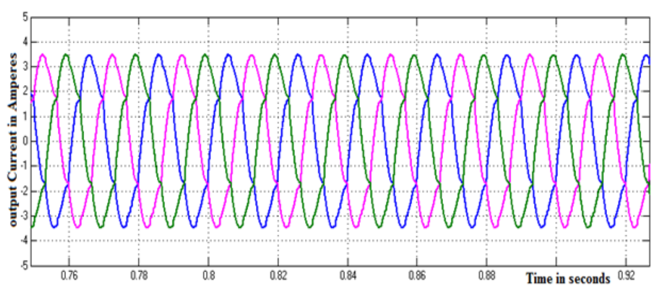

(a)

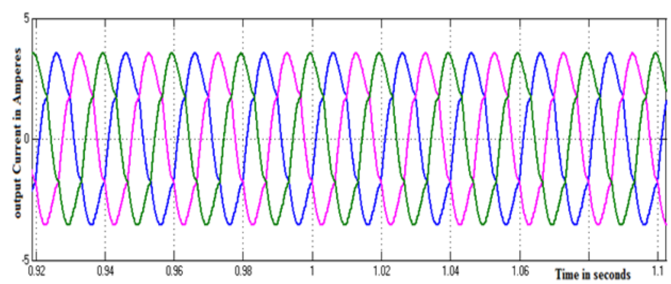

(b)

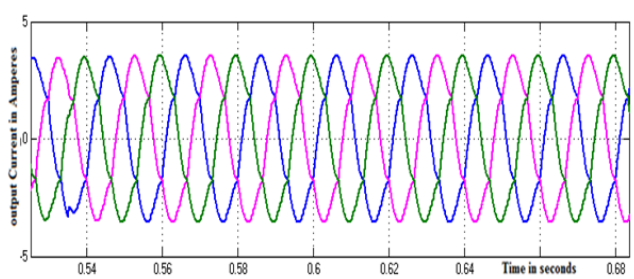

(c)

Fig. 8 Analysis of output current for (a) FOPID, (b) FLC, and (c) ANN.

Output Current THD for (a) FOPID, (b) FLC, and (c) ANN are shown in Figure 9. The Output current THD through RL load and the values for FOPID are marked as 5.21%, FLC is marked as 2.77%, and ANN is marked as 2.30%. Output Real Power for (a) FOPID, (b) FLC, and (c) ANN is shown in Figure 10. The output real power for RL load is marked for FOPID as 1980W, FLC is marked as 1983W, and ANN is marked as 1987W.

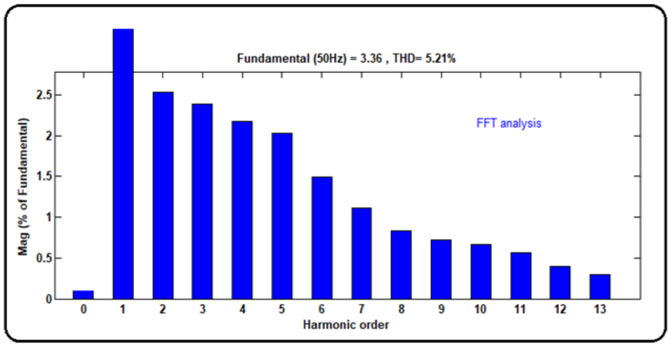

(a)

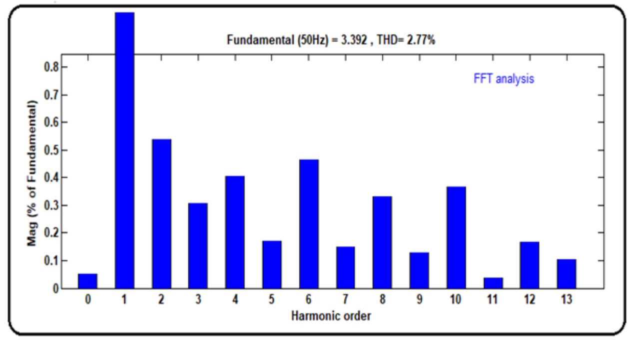

(b)

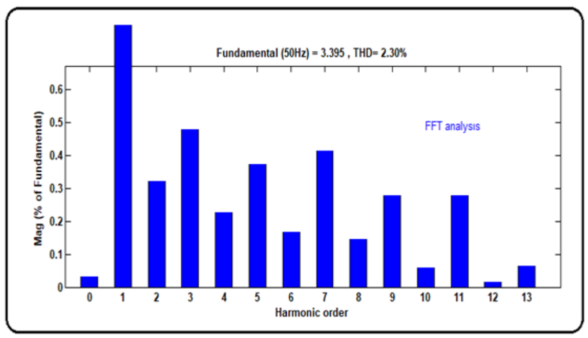

(c)

Fig. 9 Output current THD for (a) FOPID, (b) FLC, and (c) ANN.

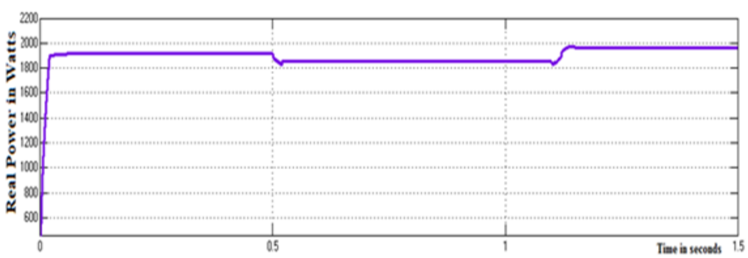

(a)

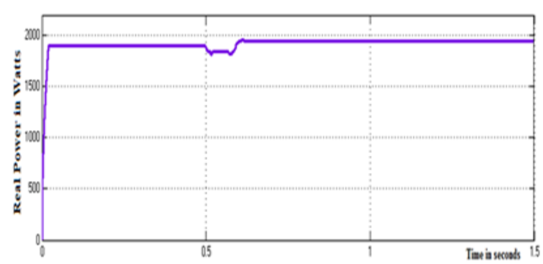

(b)

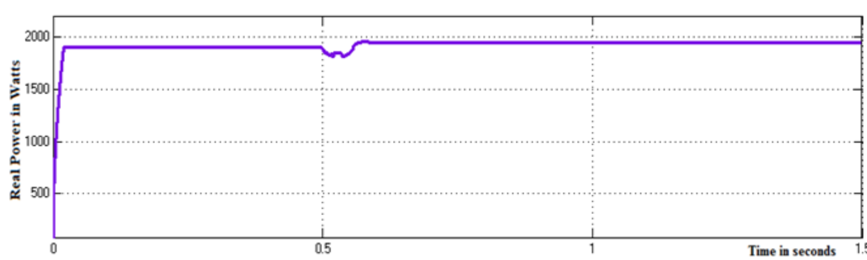

(c)

Fig. 10 Output real power for (a) FOPID, (b) FLC, and (c) ANN.

Output Reactive Power for (a) FOPID, (b) FLC, and (c) ANN is shown in Figure 11. The output reactive power for RL load is marked for FOPID as 1490VAR, FLC is marked as 1493VAR, and ANN is marked as 1513VAR.

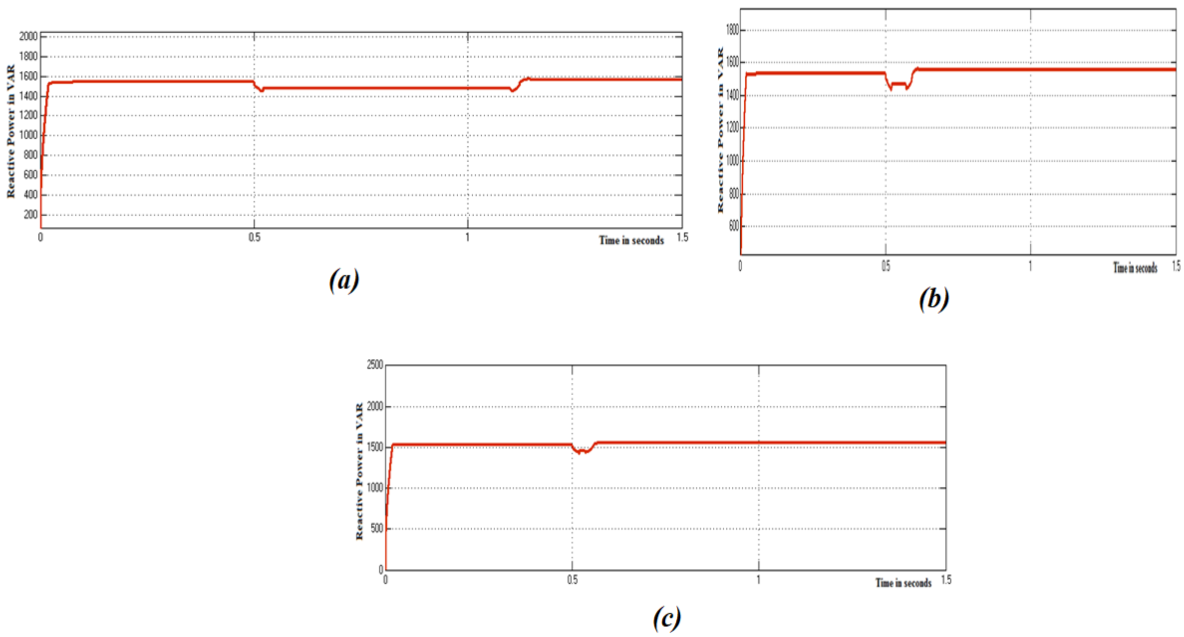

Fig. 11 Output reactive power for (a) FOPID, (b) FLC, and (c) ANN.

Table 2. Comparative analysis of time domain parameters

Controllers	Rise time (s)	Peak time (s)	Setting time (s)	Steady-State Error (V)
FOPID	1.12	1.14	1.18	3.23
FLC	0.59	0.61	0.72	1.12
ANN	0.57	0.58	0.60	0.85

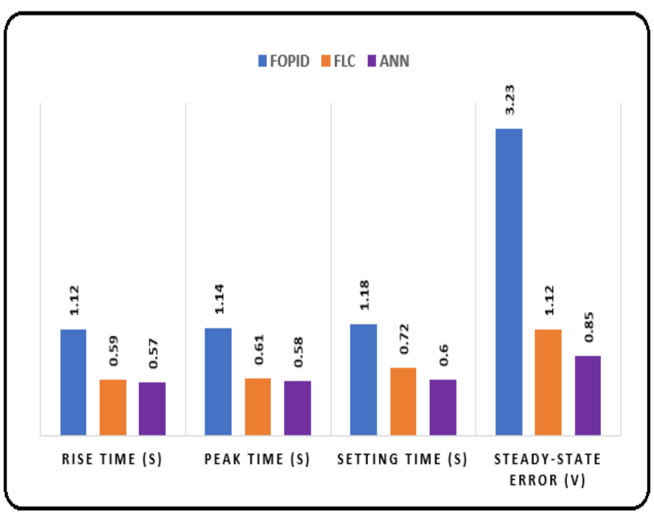

Fig. 12 Bar chart comparison of FOPID, FLC, and ANN controllers for dynamic response characteristics

Table 2 compares Time Domain Parameters for FOPID, FLC, and ANN Controllers. Figure 12 shows the Bar chart comparison of FOPID, FLC, and ANN controllers for dynamic response characteristics. Table 3 shows an evaluation of voltage and current THD for FOPID, FLC, and ANN controllers.

Table 3. Evaluation of voltage and current THD for FOPID, FLC, and ANN controllers

Controller	Voltage THD (%)	Current THD (%)
FOPID	5.11	5.21
FLC	2.96	2.77
ANN	2.20	2.30

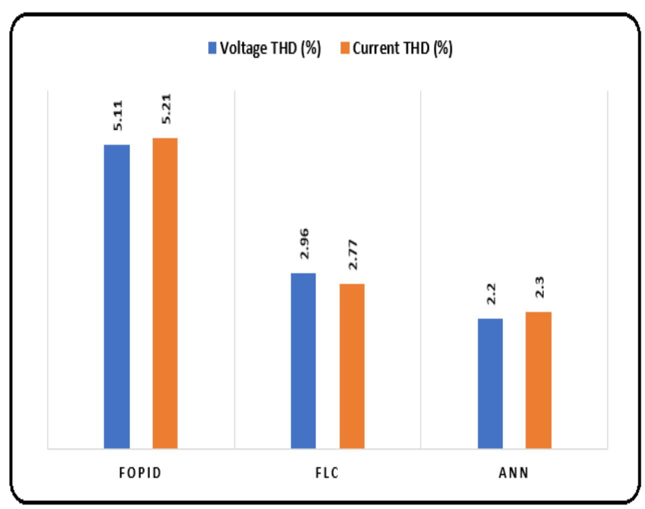

Fig. 13 Bar chart comparison of voltage THD and current THD for FOPID, FLC, and ANN controllers

Figure 13 shows the Bar chart comparison of FOPID, FLC, and ANN controllers for Voltage THD and current THD. Using the ANN controller, the dynamic response characteristics are as follows: The rise-time is condensed from 1.12s, 0.59s to 0.57s; The peak time is 1.14s, with a range of 0.61s to 0.58s when employing an ANN controller. The ANN controller reduces the settling time from 1.18s to 0.72s and 0.60s. The ANN controller reduces the steady-state error from 3.23V to 1.12V, then to 0.85V. As a result, the closed-loop ANN controller outperforms the closed-loop FOPID and Fuzzy Logic controllers in the re-boost converter with a DVR system.

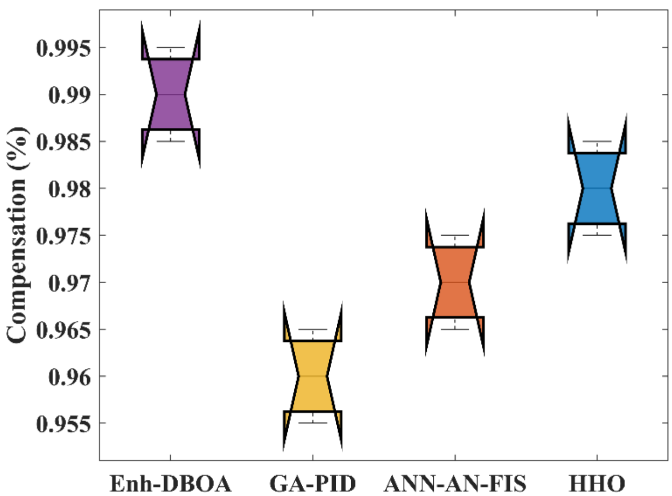

Fig. 14 Performance analysis of compensation using both proposed and existing technique

Performance analysis of compensation using both proposed and existing techniques is illustrated in Figure 14. The values for existing techniques like GA-PID, ANN-AN-FIS, and HHO are marked as 96 %, 97%, and 97.5%, and the values proposed are marked as 99%. Compared to the proposed technique, the value of the existing technique is low.

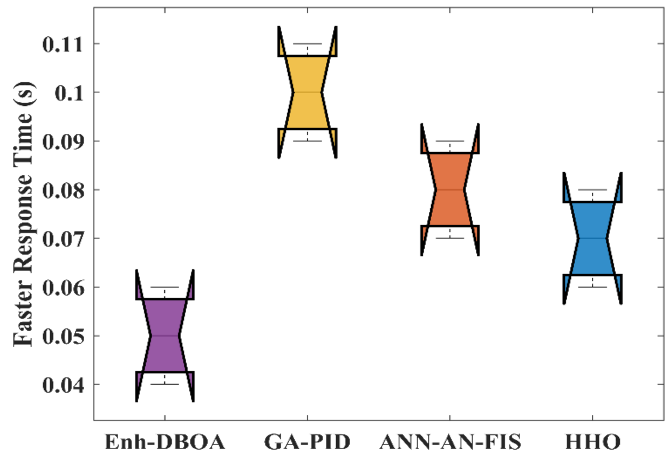

Fig. 15 Performance analysis of faster response time (s) using both proposed and existing technique

Performance analysis of Faster Response Time (s) using both proposed and existing techniques is demonstrated in Figure 15. The values for existing techniques like GA-PID, ANN-AN-FIS, and HHO are marked as 0.1 s, 0.08 s, and 0.07s, and the values proposed are marked as 0.05s. The existing technique has a lower value than the proposed technique.

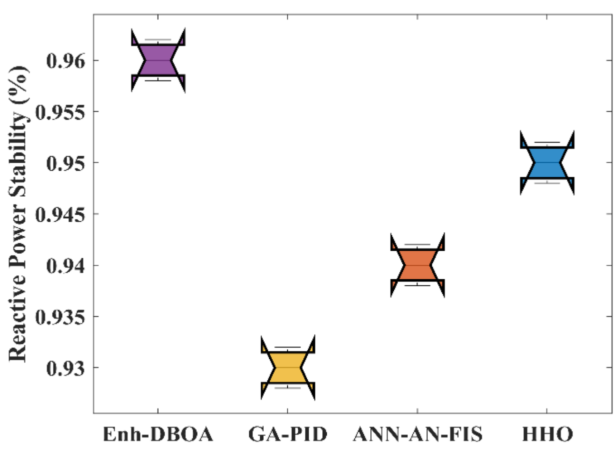

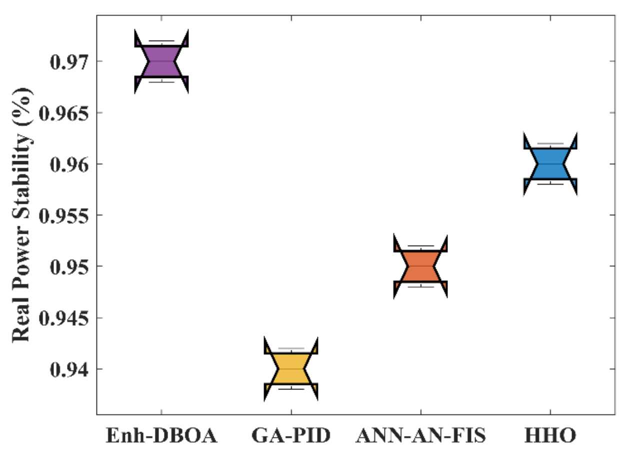

Fig. 16 Performance analysis for (a) Reactive power stability (%), and (b) Real power stability (%) using both proposed and existing technique.

Performance analysis for (a) Reactive Power Stability (%) and (b) Real Power Stability (%) using both proposed and existing techniques is shown in Figure 16. The analysis of Reactive Power stability (%) is illustrated in the figure. The values for existing techniques like GA-PID, ANN-AN-FIS, and HHO are marked as 93%, 94%, 95% and the values proposed are marked as 96%. The analysis of Real Power stability (%) is illustrated in the figure. The values for existing techniques like GA-PID, ANN-AN-FIS, and HHO are marked as 94%, 95%, 96% and the values proposed are marked as 97%. The existing technique has a lower value than the proposed technique.

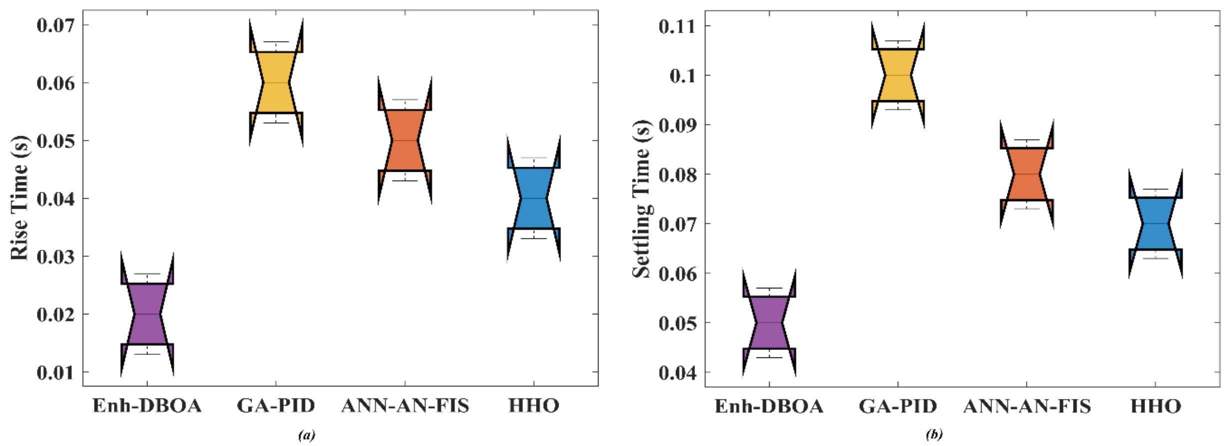

Fig. 17 Performance analysis for (a) Rise time, and (b) Setting time using both proposed and existing techniques.

Performance analysis for (a) Rise Time and (b) Setting time using both proposed and existing techniques in Figure 17. The values for existing techniques like GA-PID, ANN-AN-FIS, and HHO are marked as 0.06 s, 0.05 s, and 0.04 s, and the values proposed are marked as 0.02s.

The analysis of Real Power stability (%) is illustrated in the figure. The values for existing techniques like GA-PID, ANN-AN-FIS, and HHO are marked as 0.1s, 0.08s, and 0.07s, and the values proposed are marked as 0.05s. Compared to the existing technique, the value of the proposed technique is low.

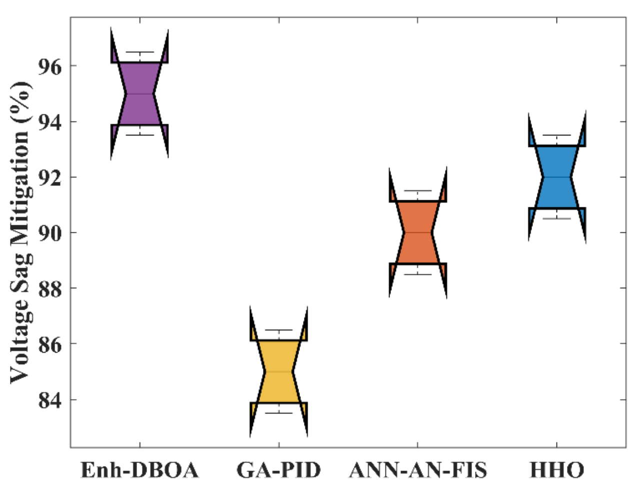

Fig. 18 Analysis of voltage sag mitigation

Voltage Sag Mitigation is shown in Figure 18. The values for existing techniques like GA-PID, ANN-AN-FIS, and HHO are marked as 85%,90%,91% and the values proposed are marked as 95%. Compared to the existing technique, the value of the proposed technique is high. Analysis of Voltage Stability is shown in Figure 19. The values for existing techniques like GA-PID, ANN-AN-FIS, and HHO are marked as 95%,96%,97%, and the values proposed are marked as 98%. The proposed technique outperforms the present technique in terms of value.

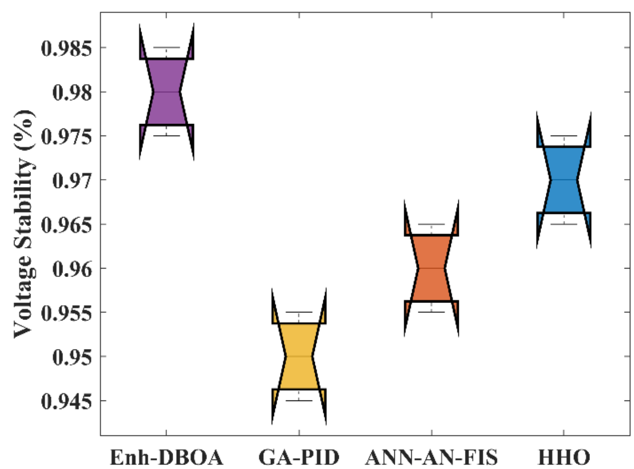

Fig. 19 Analysis of voltage stability

Evaluation of the parameter is elaborated in Table 4. The table compares four optimization methods based on important PQ and stability parameters: HHO, GA-PID, ANN-ANFIS, and Enhn-DBOA. With the fastest response time (0.05s), the highest compensation (0.99%), and the best voltage sag mitigation (95%), Enhn-DBOA performs better than any other model.

To minimize system disruptions, it also maintains exceptional reactive (0.96%) and real power stability (0.97%), as well as a quick rise time (0.02s) and settling time (0.05s). ANN-ANFIS and HHO exhibit comparable results but lag significantly below Enhn-DBOA in voltage stability, response time, and power compensation, while GA-PID performs the worst in the majority of areas. Enhn-DBOA performs better than alternative techniques, making it the best choice for improving grid-connected systems' stability and PQ.

Table 4. Evaluation of parameter

Parameters	Enhn-DBOA	GA-PID	ANN-ANFIS	HHO
Compensation (%)	0.99	0.96	0.97	0.98
Faster Response Time (s)	0.05	0.1	0.08	0.07
Reactive Power Stability (%)	0.96	0.93	0.94	0.95
Real Power Stability (%)	0.97	0.94	0.95	0.96
Rise Time (s)	0.02	0.06	0.05	0.04
Settling Time (s)	0.05	0.1	0.08	0.07
Voltage Sag Mitigation (%)	95	85	90	92
Voltage Stability (%)	0.98	0.95	0.96	0.97

4.1. Discussion on Achieved Results Compared to State-of-the-Art Techniques

The ESOA, in conjunction with the proposed Enhn-DBOA, ensures optimal tuning of FOPID, FLC, and ANN controllers for DVR systems in hybrid energy-based multi-bus grids, outperforming currently used techniques like GA-PID, ANN-ANFIS, and HHO. In comparison to GA-PID (85%), ANN-ANFIS (90%), and HHO (92%), Enhn-DBOA reduces voltage sag by 95% while obtaining better voltage stability (98%) and compensation efficiency (99%). In comparison to GA-PID (0.06s, 0.1s), ANN-ANFIS (0.05s, 0.08s), and HHO (0.04s, 0.07s), the method dramatically improves dynamic response characteristics, cutting rise time to 0.02s and settling time to 0.05s. It also reduces Total Harmonic Distortion (THD) in voltage (2.20%) and current (2.30%) and eliminates steady-state error to 0.85V, beating traditional ANN-ANFIS and HHO-based techniques. Additionally, compared to competing approaches, the system enhances the stability of real power (0.97) and reactive power (0.96). The optimization-driven DVR system is very effective in reducing voltage disturbances and improving stability in grid-connected hybrid energy systems because it guarantees faster response, better voltage regulation, and higher PQ.

5. Conclusion

In conclusion, PQ in multi-bus grid systems is greatly enhanced by the proposed hybrid-controlled DVR system optimized with the Enhn-DBOA. Regarding voltage stability, reaction time, and harmonic reduction, the comparison analysis shows that the ANN-controlled DVR system performs better than FOPID and FLC controllers. The incorporation of a Reboost converter improves the system's capacity to efficiently reduce voltage sags. Better compensation, quicker reaction, and less Total Harmonic Distortion (THD) are all guaranteed when the control parameters are adjusted for optimal DVR performance using the ESOA. The proposed method's improved performance is confirmed by the MATLAB/Simulink-based simulations, which make it a reliable way to improve PQ in distribution systems that include renewable energy sources. The performance of DVRs in extremely dynamic grid environments can be further enhanced by future research on real-time adaptive control strategies employing cutting-edge machine learning models, such as deep reinforcement learning. Including new optimization methods, including quantum-inspired algorithms, could improve control parameter tuning's effectiveness. Hardware-In-the-Loop (HIL) testing is another way to confirm that optimized DVR systems work well in practical settings. Multi-objective optimization techniques that take system dependability, energy efficiency, and economic viability into account for large-scale grid applications can also be investigated in future research. Energy management and grid resilience in smart grid environments may be further improved by the possible integration of DVR systems with blockchain-based energy trading platforms.

Reference

[1] Abdul Quawi, Y. Mohamed Shuaib, and M. Manikandan, "Power Quality Improvement Using ANN Controller for Hybrid Power Distribution Systems," *Intelligent Automation & Soft Computing*, vol. 36, no. 3, pp. 3469-3486, 2023. [CrossRef] [Google Scholar] [Publisher Link]

[2] Om Prakash Mahela et al., "Recognition of Power Quality Issues Associated with Grid Integrated Solar Photovoltaic Plant in Experimental Framework," *IEEE Systems Journal*, vol. 15, no. 3, pp. 3740-3748, 2021. [CrossRef] [Google Scholar] [Publisher Link]

[3] Muhammad Maaruf, and Muhammad Khalid, "Power Quality Control of Hybrid Wind/Electrolyzer/Fuel-Cell/Bess Microgrid," *IEEE PES Innovative Smart Grid Technologies-Asia*, Brisbane, Australia, pp. 1-5, 2021. [CrossRef] [Google Scholar] [Publisher Link]

[4] Vivek Narayanan, and Bhim Singh, "Variable Step Size Modified Clipped Least Mean Square Adaptive Control for Power Quality Improvement for a Solar PV-BS Based Microgrid with Seamless Mode Transfer Capability," *IEEE Energy Conversion Congress and Exposition*, Vancouver, BC, Canada, pp. 893-899, 2021. [CrossRef] [Google Scholar] [Publisher Link]

[5] Wesam Rohouma et al., "Adaptive Model Predictive Controller to Reduce Switching Losses for A Capacitor-Less D-STATCOM," *IEEE Open Journal of Power Electronics*, vol. 1, pp. 300-311, 2020. [CrossRef] [Google Scholar] [Publisher Link]

[6] Saeed DaneshvarDehnavi et al., "Dynamic Voltage Restorer (DVR) with A Novel Robust Control Strategy," *ISA Transactions*, vol. 121, pp. 316-326, 2022. [CrossRef] [Google Scholar] [Publisher Link]

[7] Usman Ali Khan et al., "Design and Implementation of Novel Noninverting Buck-Boost AC-AC Converter for DVR Applications," *IEEE Transactions on Industrial Electronics*, vol. 68, no. 10, pp. 9346-9357, 2021. [CrossRef] [Google Scholar] [Publisher Link]

[8] Pedram Ghavidel et al., "Fault Current Limiter Dynamic Voltage Restorer (FCL-DVR) with Reduced Number of Components," *IEEE Journal of Emerging and Selected Topics in Industrial Electronics*, vol. 2, no. 4, pp. 526-534, 2021. [CrossRef] [Google Scholar] [Publisher Link]

[9] Talada Appala Naidu et al., "Performance of DVR Using Optimized PI Controller Based Gradient Adaptive Variable Step LMS Control Algorithm," *IEEE Journal of Emerging and Selected Topics in Industrial Electronics*, vol. 2, no. 2, pp. 155-163, 2021. [CrossRef] [Google Scholar] [Publisher Link]

[10] Sabha Raj Arya et al., "Adaptive Observer for Dynamic Voltage Restorer with Optimized Proportional Integral Gains," *Chinese Journal of Electrical Engineering*, vol. 8, no. 1, pp. 38-52, 2022. [CrossRef] [Google Scholar] [Publisher Link]

[11] Roger A.D. Oliveira, and Math H.J. Bollen, "Magnification of Transients at the Voltage Dips Starting and Its Impacts on DFIG-Based Wind Power Plants," *Electric Power Systems Research*, vol. 211, 2022. [CrossRef] [Google Scholar] [Publisher Link]

[12] Omur Aydogmus, Gullu Boztas, and Resat Celikel, "Design and Analysis of a Flywheel Energy Storage System Fed by Matrix Converter as A Dynamic Voltage Restorer," *Energy*, vol. 238, 2022. [CrossRef] [Google Scholar] [Publisher Link]

[13] Ruo Huan Yang et al., "A Battery-Energy-Storage-Based DC Dynamic Voltage Restorer for DC Renewable Power Protection," *IEEE Transactions on Sustainable Energy*, vol. 13, no. 3, pp. 1707-1721, 2022. [CrossRef] [Google Scholar] [Publisher Link]

[14] R. Nasrollahi et al., "Sliding Mode Control of a Dynamic Voltage Restorer Based on PWM AC Chopper in Three-Phase Three-Wire Systems," *International Journal of Electrical Power & Energy Systems*, vol. 134, 2022. [CrossRef] [Google Scholar] [Publisher Link]

[15] Ahmed Hussain Elmetwaly et al., "Operation Control, Energy Management, and Power Quality Enhancement for a Cluster of Isolated Microgrids," *Ain Shams Engineering Journal*, vol. 13, no. 5, 2022. [CrossRef] [Google Scholar] [Publisher Link]

[16] Abdelrahman Said et al., "Alleviation of the Transients Induced in Large Photovoltaic Power Plants by Direct Lightning Stroke," *Ain Shams Engineering Journal*, vol. 14, no. 3, 2023. [CrossRef] [Google Scholar] [Publisher Link]

[17] Hatem F. Sindi et al., "Robust Control of Adaptive Power Quality Compensator in Multi-Microgrids for Power Quality Enhancement Using Puzzle Optimization Algorithm," *Ain Shams Engineering Journal*, vol. 14, no. 8, 2023. [CrossRef] [Google Scholar] [Publisher Link]

[18] Ahmed I. Omar et al., "Induced Overvoltage Caused by Indirect Lightning Strikes in Large Photovoltaic Power Plants and Effective Attenuation Techniques," *IEEE Access*, vol. 10, pp.112934-112947, 2022. [CrossRef] [Google Scholar] [Publisher Link]

[19] Muhyaddin Rawa et al., "Economical-Technical-Environmental Operation of Power Networks with Wind-Solar-Hydropower Generation Using Analytic Hierarchy Process and Improved Grey Wolf Algorithm," *Ain Shams Engineering Journal*, vol. 12, no. 3, pp. 2717-2734, 2021. [CrossRef] [Google Scholar] [Publisher Link]

[20] Ahmed I. Omar et al., "Multi-Objective Environmental Economic Dispatch of An Electricity System Considering Integrated Natural Gas Units and Variable Renewable Energy Sources," *Mathematics*, vol. 8, no. 7, pp.1-37, 2020. [CrossRef] [Google Scholar] [Publisher Link]

[21] A. Venkatesh, and P.S. Kumar, "Design of Dynamic Voltage Restorer in The Power Quality Improvement for Voltage Problems," *Applied Nanoscience*, vol. 13, no. 4, pp. 2985-2995, 2023. [CrossRef] [Google Scholar] [Publisher Link]

[22] Ch. Srivardhan Kumar, and Z. Mary Livinsa, "Development of a Novel Harris Hawks-Based Optimization Algorithm for Power Quality Enhancement in Distribution Systems Using a Dynamic Voltage Restorer," *Electrical Engineering*, vol. 105, no. 5, pp. 3105-3119, 2023. [CrossRef] [Google Scholar] [Publisher Link]

[23] Prashant Kumar et al., "A Self-Tuning ANFIS DC Link and ANN-LM Controller-Based DVR for Power Quality Enhancement," *CPSS Transactions on Power Electronics and Applications*, vol. 8, no. 4, pp. 424-436, 2023. [CrossRef] [Google Scholar] [Publisher Link]

[24] Abdallah Ben Abdelkader, Youssef Mouloudi, and Mohammed Amine Soumeur, "Integration of Renewable Energy Sources in The Dynamic Voltage Restorer for Improving Power Quality Using ANFIS Controller," *Journal of King Saud University-Engineering Sciences*, vol. 35, no. 8, pp. 539-548, 2023. [CrossRef] [Google Scholar] [Publisher Link]

[25] Muhyaddin Rawa et al., "Dynamic Voltage Restorer Under Different Grid Operating Conditions for Power Quality Enhancement with The Deployment of a PI Controller Using Gorilla Troops Algorithm," *Ain Shams Engineering Journal*, vol. 14, no. 10, 2023. [CrossRef] [Google Scholar] [Publisher Link]

[26] Aravind Chellachi Kathiresan et al., "A Versatile Control of Solar DVR For Enhanced Utilization and Power Quality Improvement in a Series-Connected Wind-Solar Farm," *IET Renewable Power Generation*, vol. 19, no. 1, 2022. [CrossRef] [Google Scholar] [Publisher Link]

[27] Jiankai Xue, and Bo Shen, "Dung Beetle Optimizer: A New Meta-Heuristic Algorithm for Global Optimization," *The Journal of Supercomputing*, vol. 79, no. 7, pp. 7305-7336, 2023. [CrossRef] [Google Scholar] [Publisher Link]

[28] Olaide Nathaniel Oyelade et al., "Ebola Optimization Search Algorithm: A New Nature-Inspired Metaheuristic Optimization Algorithm," *IEEE Access*, vol. 10, pp. 16150-16177, 2022. [CrossRef] [Google Scholar] [Publisher Link]